Supporting Information for "Exploring the iron-binding potential of the ocean using a combined pH and DOC parameterisation"

Y. Ye[1], C. Völker[1], M. Gledhill[2]

[1]Alfred Wegener Institute, Helmholz Centre for Polar and Marine Research, Bremerhaven, Germany

[2]GEOMAR Helmholtz Centre for Ocean Research, Kiel, Germany

Contents of this file

1. Tables S1 (as separate excel file)
2. Figures S1 to S7
3. Text S1

Introduction

The supporting information includes the NICA model data of iron binding to DOM (as separate excel file), DFe distributions in two previous studies (Figure S1 and S2) the GLODAP pH distribution (Figure S3) and the difference between GLODAP and NorESM-ME simulated present-day pH (Figure S4), changes in *logk* (Figure S5) and deep water DFe (Figure S6) caused by future climate driven changes in pH, and the relationship between

---

Corresponding author: Y. Ye, Department of Marine Biogeoscience, Alfred Wegener Institute, Helmholz Centre for Polar and Marine Research, Am Handelshafen 12, 27570 Bremerhaven, Germany (Ying.Ye@awi.de)

February 26, 2020, 11:17pm

$log\alpha$, DOC and DFe in the standard model run (Figure S7). A detailed description of the discrepancy between the GLODAP and NorESM-ME simulated present-day pH is given in Text S1.

The NICA model was used in combination with the speciation program visual Minteq (Visual MINTEQ version 3.0., https://vminteq.lwr.kth.se/) to model iron binding to DOM over a range of iron concentrations (0.1–2 μmol m^{-3}), dissolved organic carbon concentrations (40–100 mmol m^{-3}) and pH values (7.2–8.2, free scale). All calculations were done for 20°C and a salinity of 35 PSU. Model output includes concentrations of iron hydroxide species, free iron ions and iron bound to organic matter.

Text S1: pH data used in this study

Two pH fields have been used in this study to calculate the apparent conditional stability constants: GLODAP pH data (Fig. S3) for the standard run R_{stand}, and pH data from NorESM1-ME for the future scenario RCP8.5 (Taylor et al., 2012) for R_{ph}. Both of the pH fields have been interpolated to our model grid.

In Sec. 3.3, we discuss the model response to pH change in one high emission scenario. Change of $logk$, DFe and α_{FeL} in R_{ph} compared to R_{stand} should be interpreted as the result from the future pH trend. It is however important to point out that the pH difference between R_{ph} and R_{stand} is not only caused by changing environmental conditions in RCP8.5 scenario but also by the discrepancy between the GLODAP data and the present-day pH field simulated by NorESM-ME (Fig. S4).

The surface pH from the NorESM-ME present-day simulation (not shown) shows a similar pattern to GLODAP data with higher values in gyres and but the variability is lower (NorESM-ME pH values range between 7.8 and 8.2 and GLODAP between 7.8 and 8.5). pH values in the intermediate and deep water from the NorESM-ME present-day simulation however, is significantly higher in the North Pacific (up to 0.4 pH units) and slightly higher in the Southern Ocean and Indian Ocean. This accounts for the pH increase from GLODAP to NorESM-ME future simulation (Fig. 5B and C) and has an effect on the deep distribution of DFe. This could affect the surface DFe concentration by upwelling and mixing, and thus affect the response of α_{FeL} to pH change. Therefore in this study, we do not interpret the result of R_{ph} as the response to pH decrease or ocean acidification but to the relative pH change between NorESM-ME pH of RCP8.5 and GLODAP pH data. In a future study, we will predict changes in the iron-binding

potential of the world's ocean with ocean acidification by simulating the present-day pH field in our model, validating it with GLODAP data and calculating the future pH under defined climate conditions.

References

Taylor, K. E., Stouffer, R. J., & Meehl, G. A. (2012). An Overview of CMIP5 and the Experiment Design. *Bulletin of the American Meteorological Society*, *93*(4), 485–498. doi: 10.1175/BAMS-D-11-00094.1

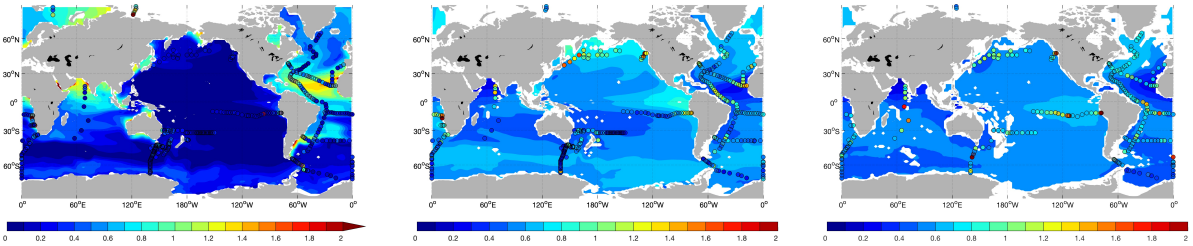

A B C

Figure S1. Modelled (R_{constL}) and measured (GEOTRACES IDP2017) DFe (μmol m^{-3}), averaged between 0–100 (A), 500–1000 (B) and 2000–3000 m (C).

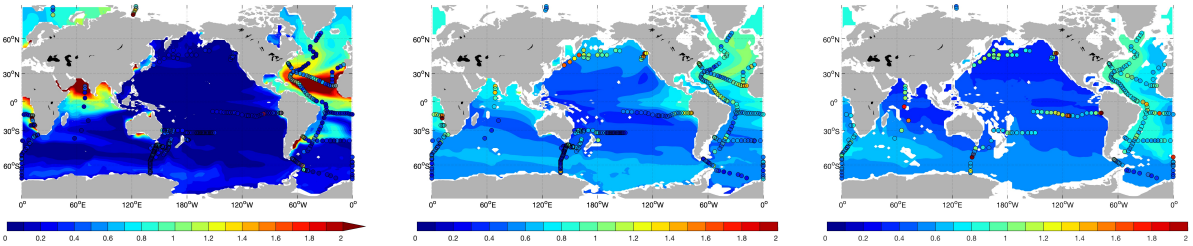

A B C

Figure S2. Modelled (R_{progL}) and measured (GEOTRACES IDP2017) DFe (μmol m^{-3}), averaged between 0–100 (A), 500–1000 (B) and 2000–3000 m (C).

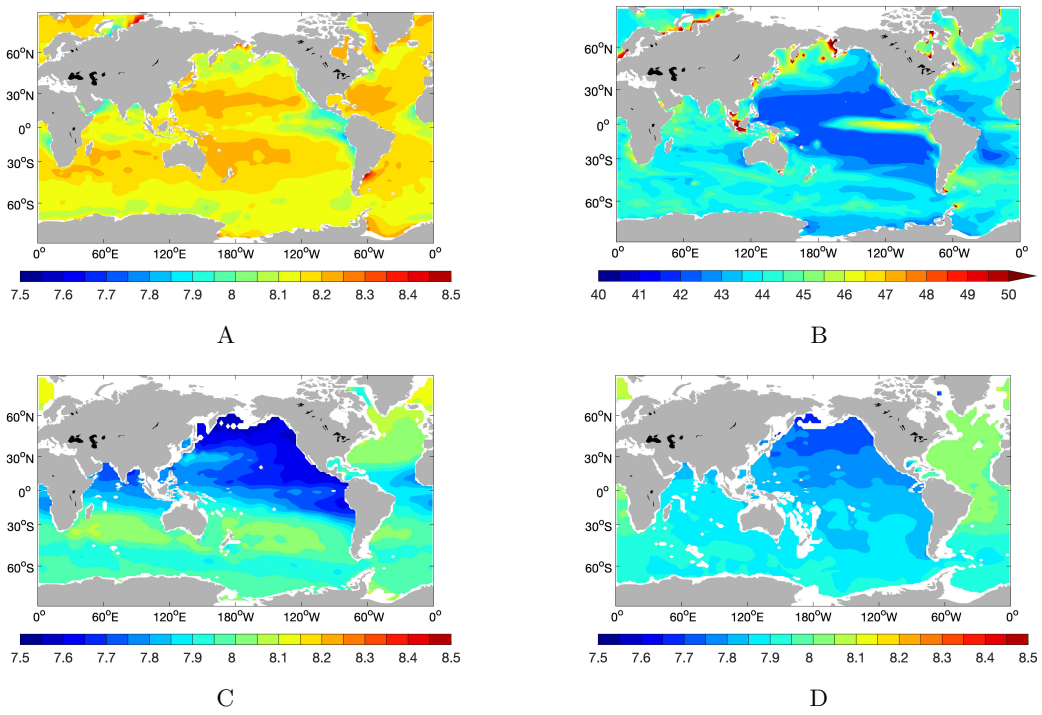

Figure S3. GLODAP pH interpolated to our model grid, averaged between 0–100 (A), 500–1000 (C) and 2000–3000 m (D), and modelled DOC concentration (mmol C m^{-3}) averaged between 0–100 m (B). Below the surface ocean, a uniform DOC distribution around 42 mmol C m^{-3} is found in the model representing the refractory fraction of DOC.

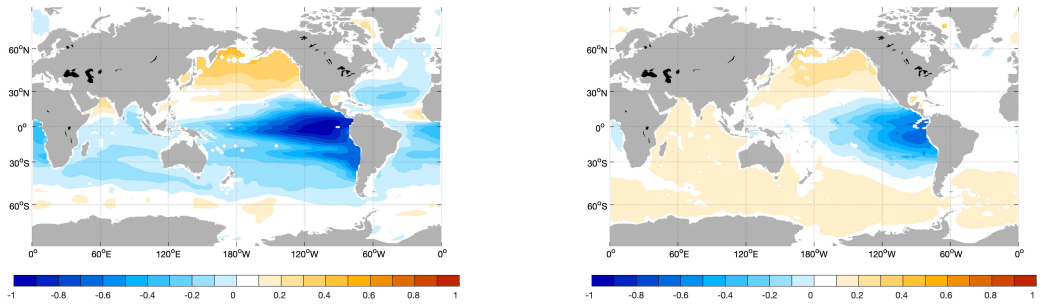

Figure S4. Difference between pH simulated by NorESM-ME for 2005 and GLODAP pH, averaged between 500–1000 (A) and 2000–3000 m (B).

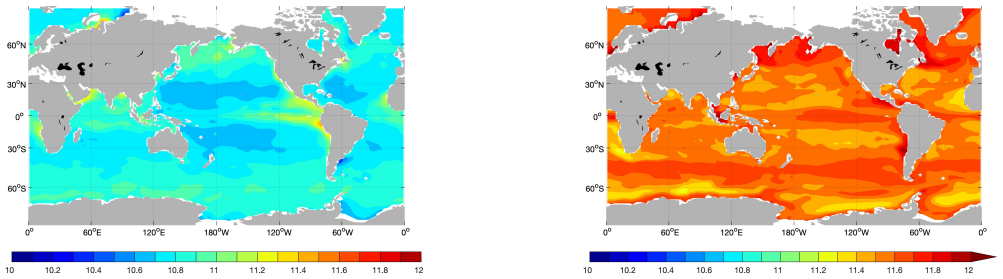

A B

Figure S5. Apparent conditional stability constant $logk1$ in R_{stand} (A) and R_{ph} (B) averaged for the upper 100 m. $logk2$ is not shown since its difference to $logk1$ is constant at 2.67 (Sec. 2.3).

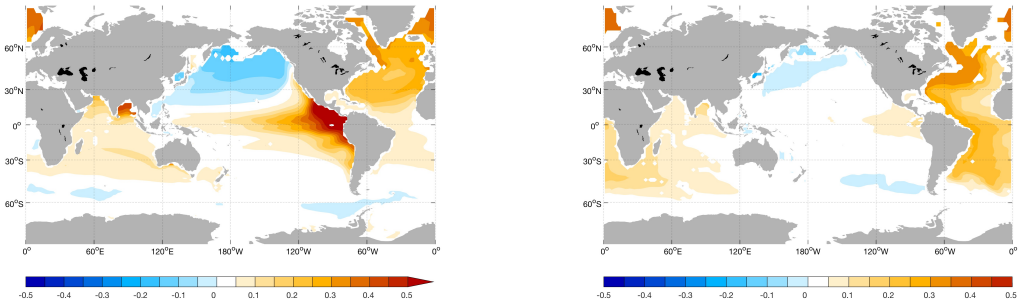

A B

Figure S6. Change of DFe (μmol m^{-3}) in R_{ph} relative to R_{stand} averaged for the vertical layer 500–1000 m (A) and between 2000–3000 m(B).

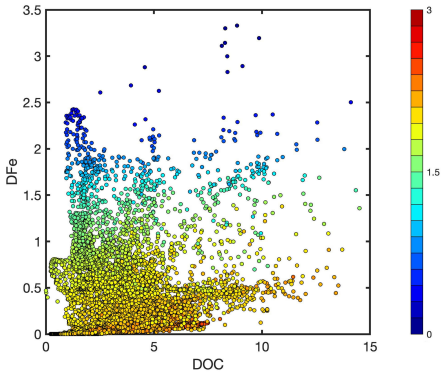

Figure S7. Modelled DFe (μmol m^{-3}), DOC (mmol m^{-3}) ~~a~~and $log(\alpha)$ (colours of the dots) at the surface in R_{stand}. Only the labile fraction of DOC is considered here.